Supporting Information

Porous Nickel-Iron Selenide Nanosheets as Highly Efficient Electrocatalysts for Oxygen Evolution Reaction

Zhaoyang Wang, Jiantao Li, Xiaocong Tian, Xuanpeng Wang, Yang Yu, Kwadwo Asare Owusu, Liang He, Liqiang Mai**

State Key Laboratory of Advanced Technology for Materials Synthesis and Processing,
Wuhan University of Technology, Wuhan 430070, Hubei (P.R. China)
E-mail: mlq518@whut.edu.cn; hel@whut.edu.cn
Fax: +86-27-87644867; Tel: +86-27-87467595

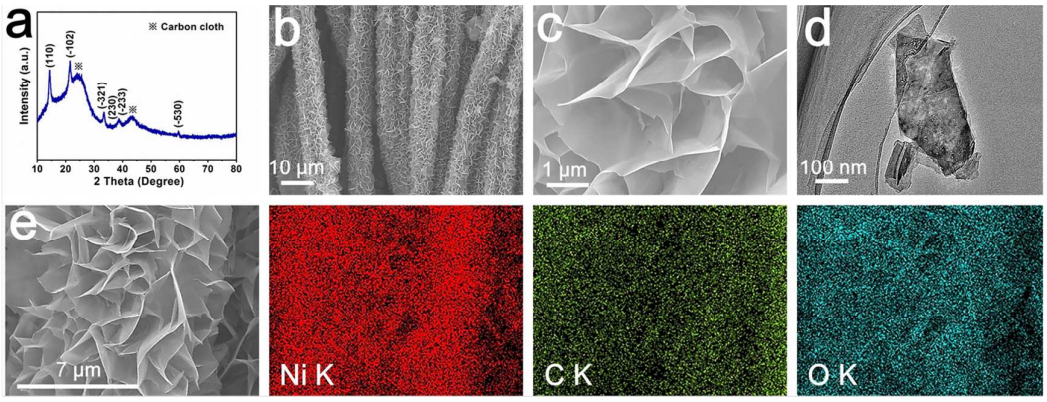

Figure S1. XRD pattern (a), SEM images (b, c), TEM image (d), SEM image and elemental mapping images (e) of the ultrathin Ni-based nanosheet precursor.

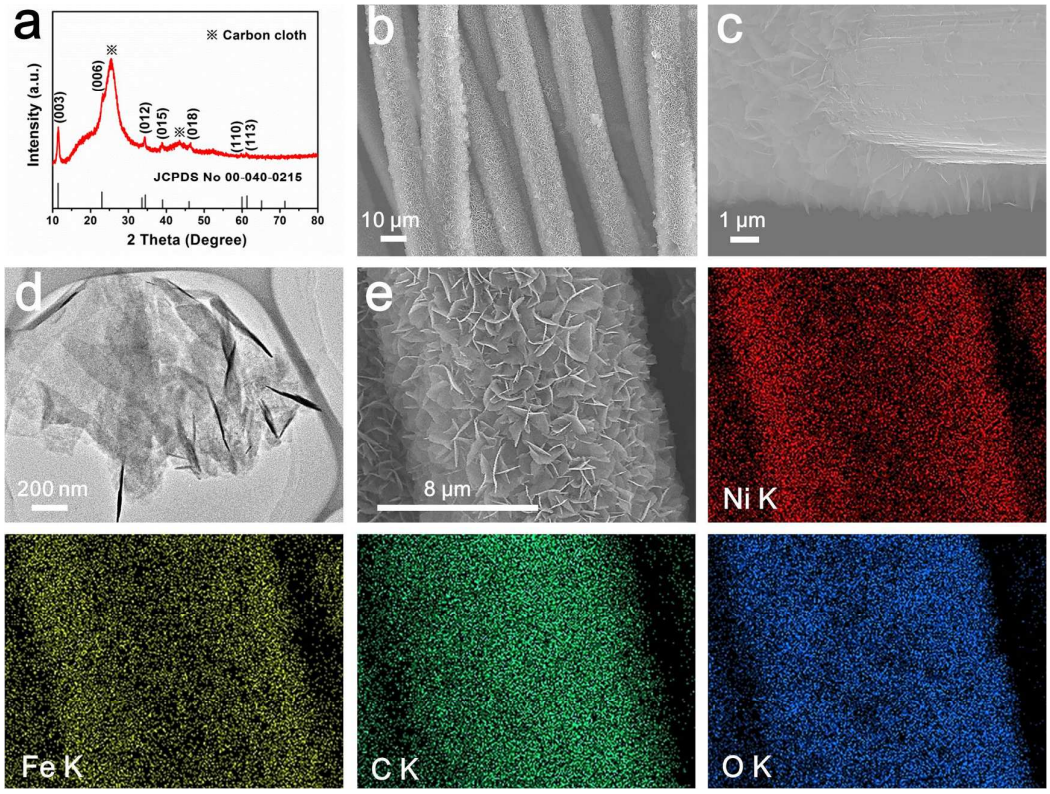

Figure S2. XRD pattern (a), SEM images (b, c), TEM image (d), SEM image and elemental mapping images (e) of the ultrathin NiFe-based nanosheet precursor.

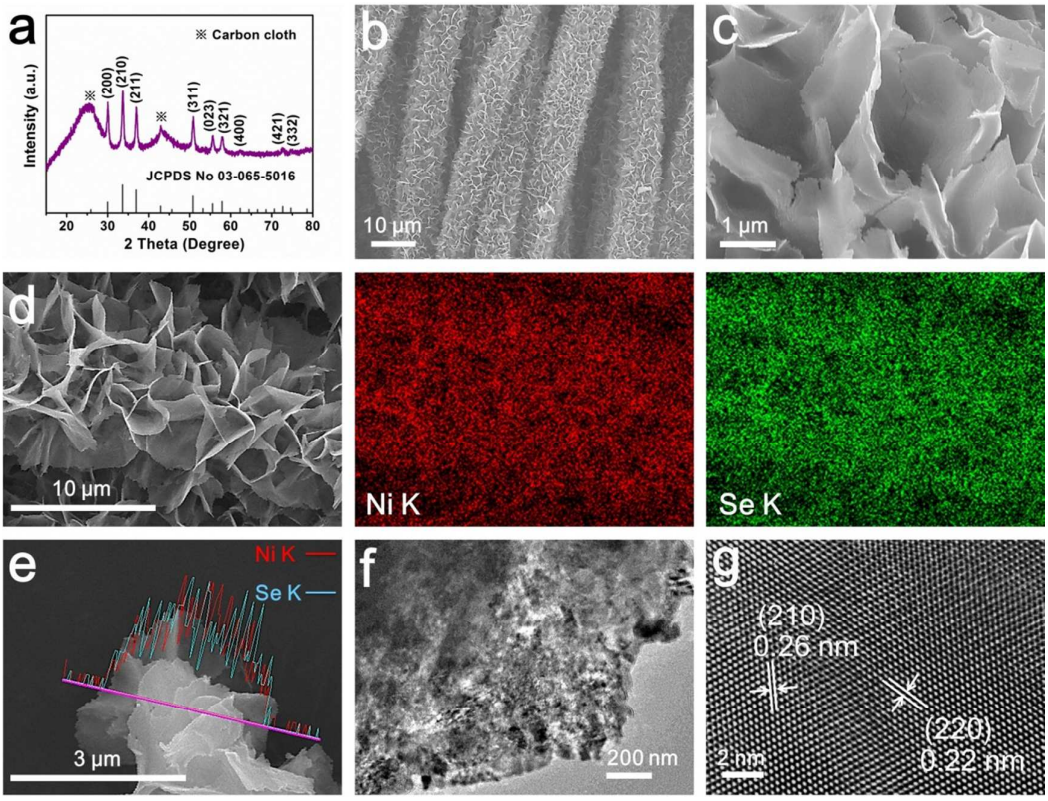

Figure S3. XRD pattern (a), SEM images (b, c), elemental mapping images (d), EDS line scans (e), TEM image (f), and HRTEM image (g) of the porous $NiSe_2$ nanosheets.

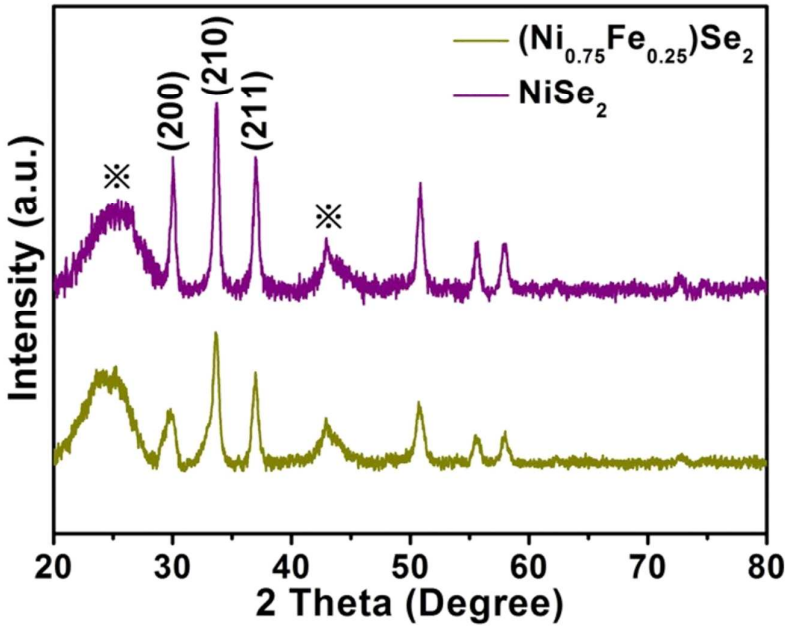

Figure S4. XRD patterns of the porous $(Ni_{0.75}Fe_{0.25})Se_2$ nanosheets, and the porous $NiSe_2$ nanosheets.

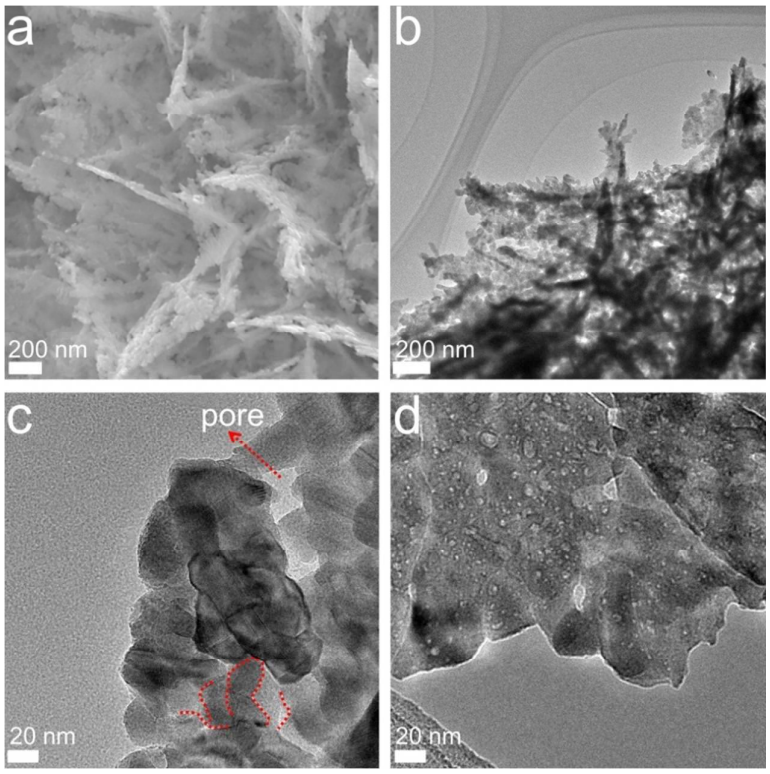

Figure S5. High-resolution SEM image (a), TEM image (b), and (c) HRTEM image of the porous $(Ni_{0.75}Fe_{0.25})Se_2$ nanosheet. TEM image (d) of the porous $NiSe_2$ nanosheet.

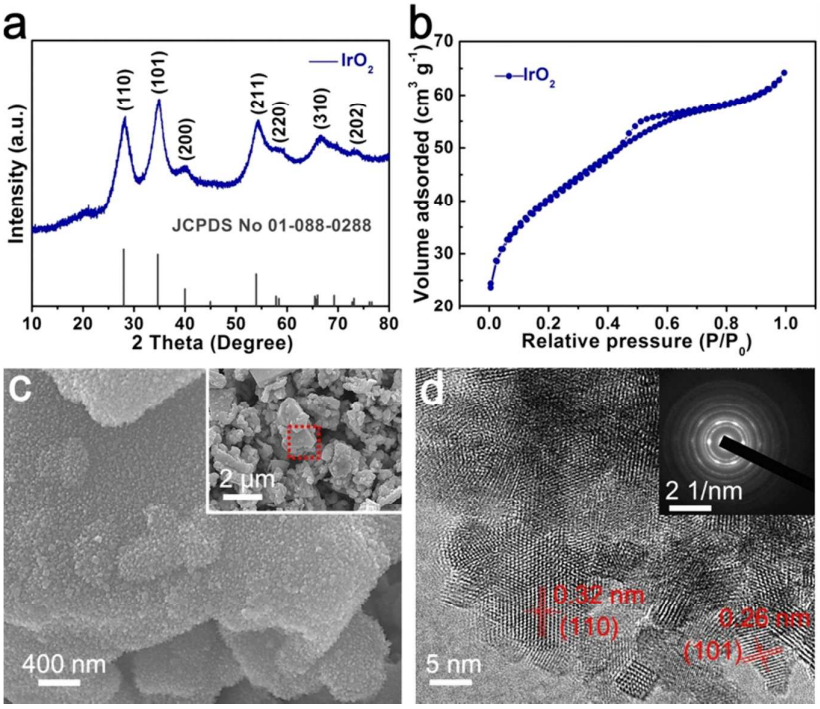

Figure S6. XRD pattern (a), Nitrogen adsorption-desorption isotherm (b), SEM images (c), HRTEM image and SAED pattern (d) of IrO_2 catalyst.

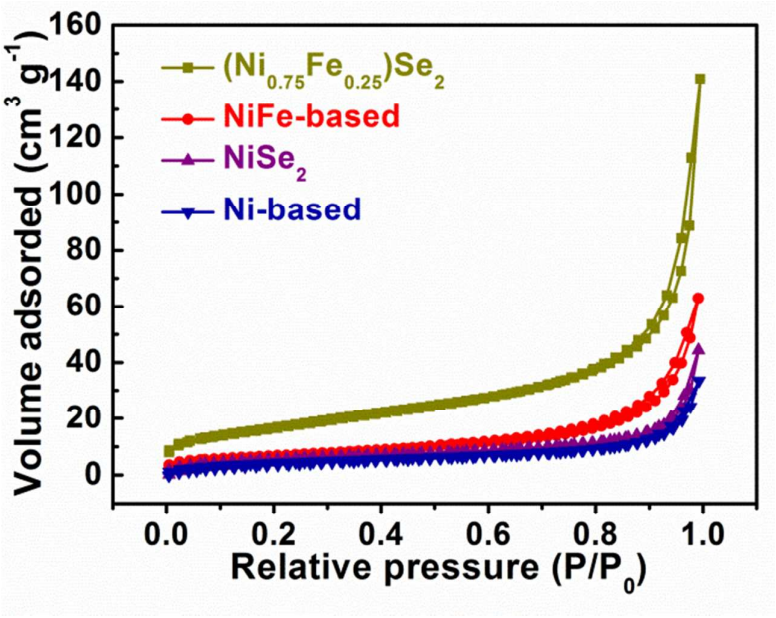

Figure S7. Nitrogen adsorption-desorption isotherm of porous $(Ni_{0.75}Fe_{0.25})Se_2$ nanosheets, NiFe-based nanosheet precursor, porous $NiSe_2$ nanosheets, and Ni-based nanosheet precursor.

Table S1. ICP results of NiFe-based nanosheet precursor, porous (NiFe)Se nanosheets, and porous $NiSe_2$ nanosheets.

Sample	Ni (wt.%)	Fe (wt.%)	Se (wt.%)	Element molar ratios
NiFe-based	5.204	1.712	NA	2.89:1
(NiFe)Se	3.749	1.224	14.782	2.91:1:8.54
$NiSe_2$	1.091	NA	3.236	1:2.21

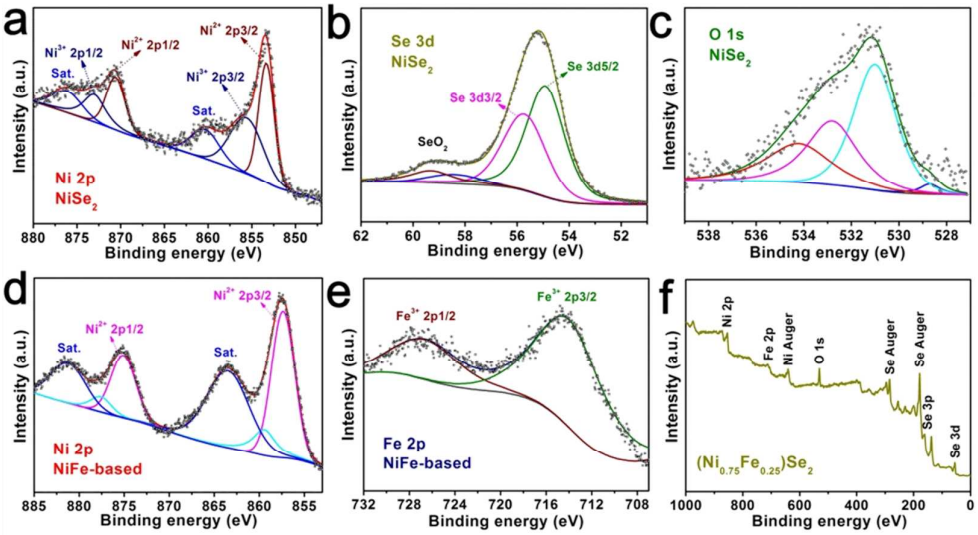

Figure S8. High-resolution (a) Ni 2p, (b) Se 3d, and (c) O 1s XPS spectra for the porous $NiSe_2$ nanosheets. High-resolution (d) Ni 2p and (e) Fe 2p XPS spectra for the NiFe-based precursor. XPS survey spectrum for the (f) porous $(Ni_{0.75}Fe_{0.25})Se_2$ nanosheets.

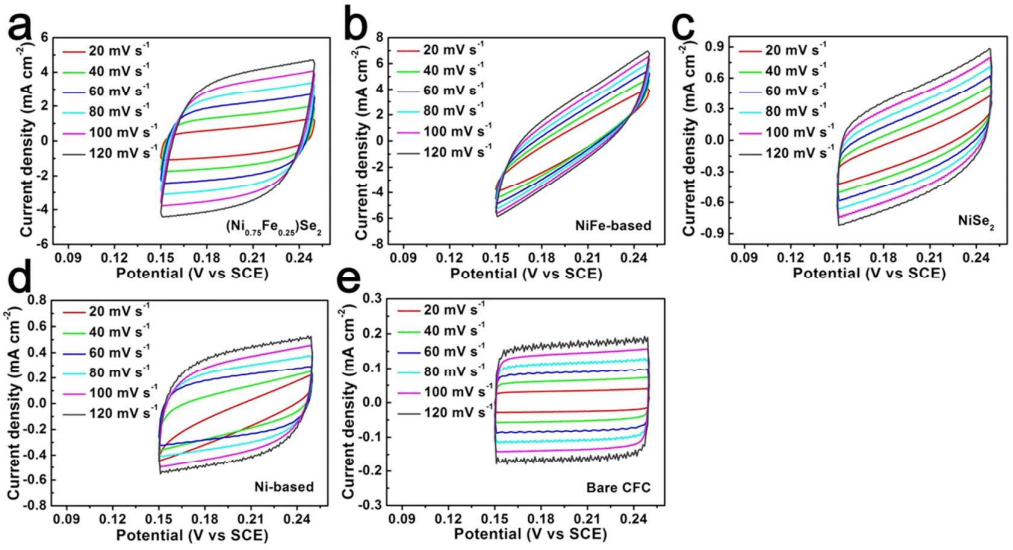

Figure S9. The double-layer capacitance measurements of the obtained $(Ni_{0.75}Fe_{0.25})Se_2$ (a), NiFe-based precursor (b), $NiSe_2$ (c), Ni-based precursor (d) and carbon fiber cloth (e) samples.

The ECSA was determined by measuring the capacitive current associated with double-layer charging from the cyclic voltammetry (CV) curves at different scan rates. A linear slope is obtained from the plot of the differences in the charging current density (J_a-J_c) at 0.2 V (*vs.* saturated calomel electrode) against the scan rate. The linear slope is twice of the double-layer capacitance (C_{dl}). The CV of the samples were tested using a three electrode system in a 0.15-0.25 V potential window with the scan rates from 20 mV s^{-1} to 120 mV s^{-1}.

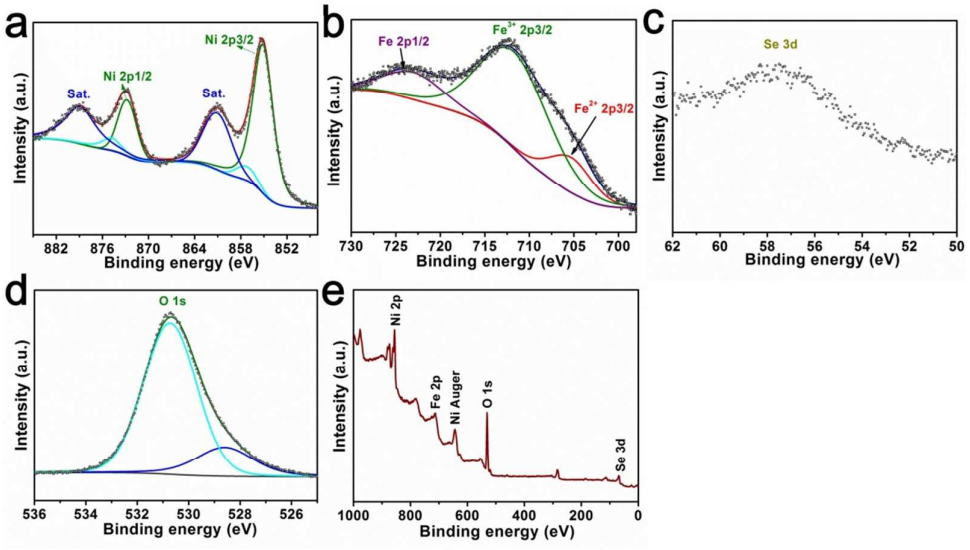

Figure S10. XPS spectra in the (a) Ni 2p, (b) Fe 2p, (c) Se 3d, and (d) O 1s regions for the $(Ni_{0.75}Fe_{0.25})Se_2$ catalyst after OER electrolysis in 1 M KOH. XPS survey spectrum of the (e) post-OER $(Ni_{0.75}Fe_{0.25})Se_2$ catalyst.

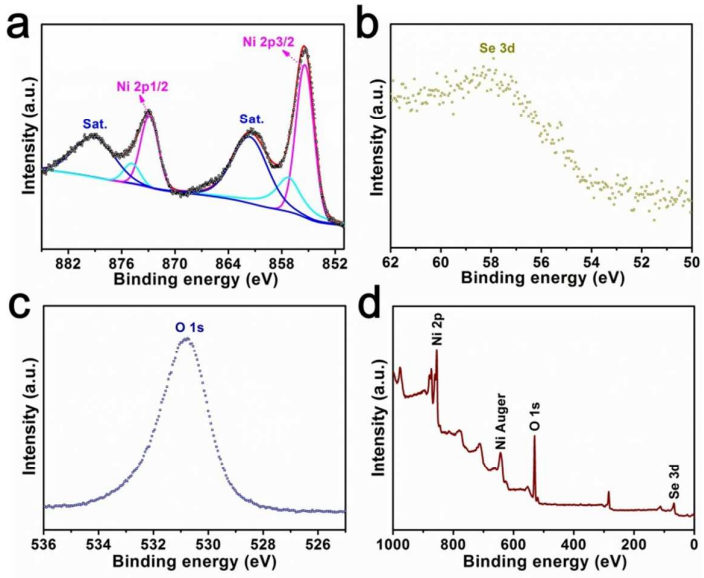

Figure S11. XPS spectra in the (a) Ni 2p, (b) Se 3d, and (c) O 1s regions for the $NiSe_2$ catalyst after OER electrolysis in 1 M KOH. XPS survey spectrum of the (d) post-OER $NiSe_2$ catalyst.

Table S2. ICP results for the porous (NiFe)Se nanosheets and porous $NiSe_2$ nanosheets after OER electrolysis.

Sample	Ni (wt.%)	Fe (wt.%)	Se (wt.%)	Element molar ratios
(NiFe)Se	0.792	0.256	0.572	2.94:1:1.58
$NiSe_2$	1.465	NA	0.937	1:0.48

Table S3. The composition analysis from deconvolution of XPS spectra before and after OER test.

Catalysts $(Ni_{0.75}Fe_{0.25})Se_2$	Element analysis (At.%)		
	Ni	Fe	Ni : Fe
Before OER	23.57	8.12	2.90 : 1
After OER	20.25	7.08	2.86 : 1

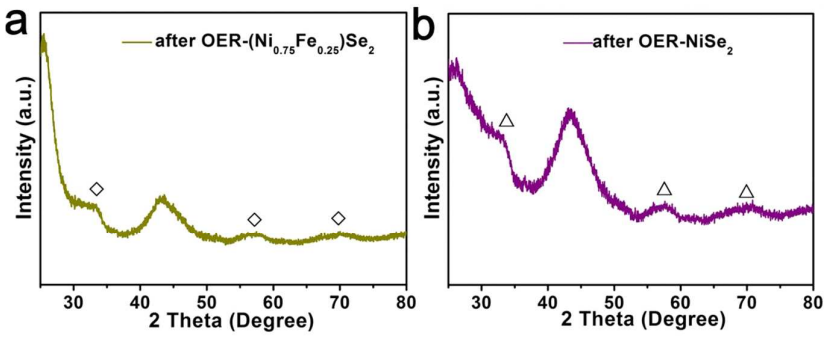

Figure S12. XRD patterns of the $(Ni_{0.75}Fe_{0.25})Se_2$ (a) and $NiSe_2$ (b) after OER electrolysis.

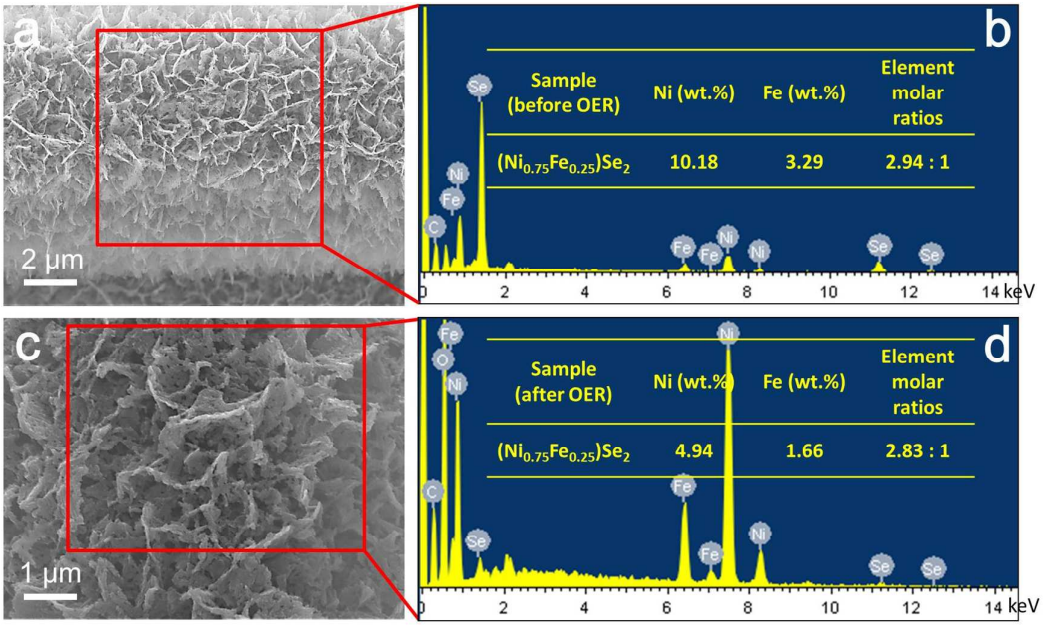

Figure S13. SEM image (a) and EDS spectrum (b) for the $(Ni_{0.75}Fe_{0.25})Se_2$ catalyst before OER electrolysis, SEM image (c) and EDS spectrum (d) for the $(Ni_{0.75}Fe_{0.25})Se_2$ catalyst after OER electrolysis.

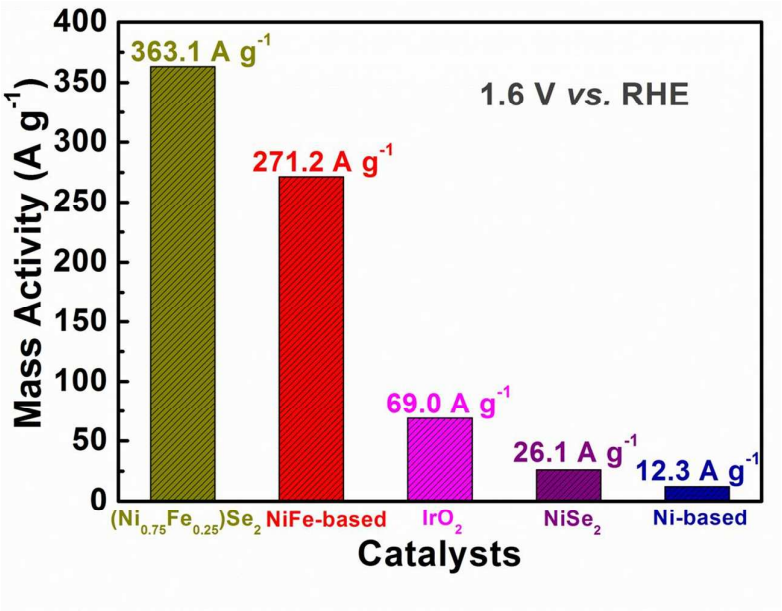

Figure S14. Mass activity based on the weight of the $(Ni_{0.75}Fe_{0.25})Se_2$, NiFe-based nanosheet precursor, $NiSe_2$, Ni-based nanosheet precursor, and IrO_2 catalysts at 1.6 V *vs.* reversible hydrogen electrode (RHE).

Table S4. The R_s and R_{ct} values of the samples from EIS spectra (Figure 5) simulated using the corresponding equivalent circuit.

Sample	R_s (Ω)	R_1 (Ω)	R_{ct} (Ω)
$(Ni_{0.75}Fe_{0.25})Se_2$	3.67	0.21	0.78
NiFe-based	3.65	0.19	1.22
$NiSe_2$	5.05	0.39	3.39
Ni-based	4.69	1.03	21.75

Table S5. Comparison of OER activity for the $(Ni_{0.75}Fe_{0.25})Se_2$/CFC with some reported non-noble metal catalysts in alkaline electrolytes.

Catalysts	Mass loading mg cm^{-2}	Current density (mA cm^{-2})	Overpotential (mV)	Tafel sloper (mV dec^{-1})	Double layer capacitance (mF cm^{-2})	Electrolyte	Substrate	Reference
$(Ni_{0.75}Fe_{0.25})Se_2$ nanosheets	1.5	35	255	47.2	30.2	1 M KOH	Carbon cloth	This work
$NiCo_2S_4$ nanowires	0.4	20	280	89	31.5	1 M KOH	Carbon cloth	(1)
NiSe nanowires	2.8	20	270	64	NA	1 M KOH	Ni foam	(2)
Ni_3N nanosheets	--	10	256	41	NA	1 M KOH	Carbon cloth	(3)
Co_4N nanowires	0.8	10	257	44	365.5	1 M KOH	Carbon cloth	(4)
Co_3O_4/C nanowires	0.2	10	290	70	209.7	0.1 M KOH	Cu foil	(5)
CoP nanorods/C	0.7	10	320	71	NA	1 M KOH	Glassy carbon	(6)
$CoNi(OH)_x$ nanotubes	0.7	10	280	77	NA	1 M KOH	Cu foil	(7)
$(Ni, Co)_{0.85}Se$ nanotubes	5.0	10	255	79	22.9	1 M KOH	Carbon cloth	(8)
$Zn_xCo_{3-x}O_4$ nanowires	1.0	10	320	51	150.7	1 M KOH	Ti foil	(9)
FeOOH/Co /FeOOH nanotubes	0.5	21	250	32	306.4	1 M NaOH	Ni foam	(10)

Additional references:

(1) Liu, D.; Lu, Q.; Luo, Y.; Sun, X.; Asiric, A. M. $NiCo_2S_4$ Nanowires Array as an Efficient Bifunctional Electrocatalyst for Full Water Splitting with Superior Activity. *Nanoscale* **2015**, 7, 15122-15126.

(2) Tang, C.; Cheng, N.; Pu, Z.; Xing, W.; Sun, X. NiSe Nanowire Film Supported on Nickel Foam: An Efficient and Stable 3D Bifunctional Electrode for Full Water Splitting. *Angew. Chem. Int. Ed.* **2015**, 54, 9351-9355.

(3) Xu, K.; Chen, P.; Li, X.; Tong, Y.; Ding, H.; Wu, X.; Chu, W.; Peng, Z.; Wu, C.; Xie, Y. Metallic Nickel Nitride Nanosheets Realizing Enhanced Electrochemical Water Oxidation. *J. Am. Chem. Soc.* **2015**, 137, 4119-4125.

(4) Chen, P.; Xu, K.; Fang, Z.; Tong, Y.; Wu, J.; Lu, X.; Peng, X.; Ding, H.; Wu, C.; Xie, Y. Metallic Co_4N Porous Nanowire Arrays Activated by Surface Oxidation as Electrocatalysts for the Oxygen Evolution Reaction. *Angew. Chem. Int. Ed.* **2015**, 54, 14710-14714.

(5) Ma, T. Y.; Dai, S.; Jaroniec, M.; Qiao, S. Z. Metal-Organic Framework Derived Hybrid Co_3O_4-Carbon Porous Nanowire Arrays as Reversible Oxygen Evolution Electrodes. *J. Am. Chem. Soc.* **2014**, 136, 13925-13931.

(6) Chang, J.; Xiao, Y.; Xiao, M.; Ge, J.; Liu, C.; Xing, W. Surface Oxidized Cobalt-Phosphide Nanorods as an Advanced Oxygen Evolution Catalyst in Alkaline Solution. *ACS Catal.* **2015**, 5, 6874-6878.

(7) Li, S.; Wang, Y.; Peng, S.; Zhang, L.; Al-Enizi, A. M.; Zhang, H.; Sun, X.; Zheng, G. Co–Ni-Based Nanotubes/Nanosheets as Efficient Water Splitting Electrocatalysts. *Adv. Energy Mater.* **2015**, 6, DOI: 10.1002/aenm.201501661.

(8) Xia, C.; Jiang, Q.; Zhao, C.; Hedhili, M. N.; Alshareef, H. N. Selenide-Based Electrocatalysts and Scaffolds for Water Oxidation Applications. *Adv. Mater.* **2015**, 28, 77-85.

(9) Liu, X.; Chang, Z.; Luo, L.; Xu, T.; Lei, X.; Liu, J.; Sun, X. Hierarchical $Zn_xCo_{3-x}O_4$ Nanoarrays with High Activity for Electrocatalytic Oxygen Evolution. *Chem. Mater.* **2014**, 26, 1889-1895.

(10) Feng, J.; Xu, H.; Dong, Y.; Ye, S.; Tong, Y.; Li, G. FeOOH/Co/FeOOH Hybrid Nanotube Arrays as High-Performance Electrocatalysts for the Oxygen Evolution Reaction. *Angew. Chem. Int. Ed.* **2016**, 55, 3758-3762.